HNPS Advances in Nuclear Physics

Vol 15 (2006)

HNPS2006

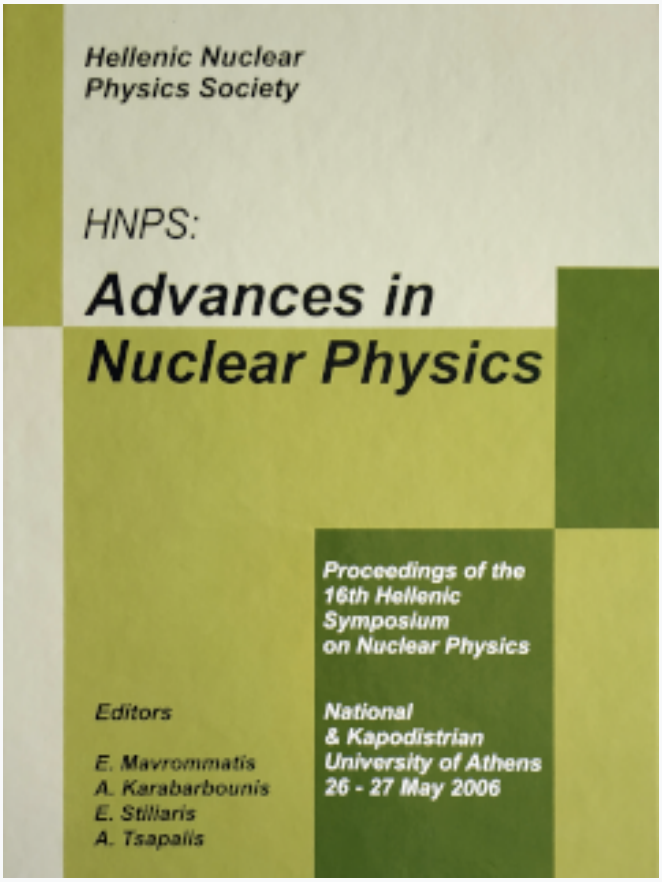

The critical point of Bootstrap and Lattice QCD

N. G. Antoniou, F. K. Diakonos, A. S. Kapoyannis

doi: 10.12681/hnps.2643

The critical point of Bootstrap and Lattice QCD

N.G. Antoniou[a], F.K. Diakonos[a] and A.S. Kapoyannis[a] *

[a]Department of Physics, University of Athens, 15771 Athens, Greece

It is shown that the hadronic matter formed at high temperatures, according to the prescription of the statistical bootstrap principle, develops a critical point at nonzero baryon chemical potential. The location of the critical point is evaluated with the use of lattice QCD pressure.

1. Introduction

Quantum Chromodynamics predicts a phase transition between the quark and the hadronic matter. This transition is of first order at higher baryon densities and lower temperatures and a smooth crossover at low densities and higher temperatures. At the end of the first order transition a critical point of second order is predicted [1]. The existence of such an endpoint is also predicted by the thermodynamics of interacting hadronic matter (Statistical Bootstrap) [2] and with the use of recent Lattice calculation the determination of its location is possible [3].

2. Hadronic thermodynamics of Statistical Bootstrap

The Statistical Bootstrap (SB) [4] is based on the hypothesis that the strong interactions can be simulated by the presence of hadronic clusters. In the context of SB the strongly interacting hadron gas is replaced by a non-interacting infinite-component cluster gas. The hadronic states of clusters are listed in a mass spectrum $\tilde{\rho}(m)$. In the bootstrap scheme clusters are composed of clusters described by the same mass spectrum. This scheme proceeds until clusters are reached which are composed of constituents no further divided. These constituents are the *input* hadrons and all the known hadronic particles can be identified to belong to this category.

The asymptotic solution for the mass spectrum is found to rise *exponentially*: $\tilde{\rho}(m) \overset{m\to\infty}{\longrightarrow} \sim m^{-\alpha} \exp[m\beta^*(\{\lambda\})]$, where β^* is the inverse maximum temperature allowed for hadronic matter which depends on the existing fugacities $\{\lambda\}$ and α is an exponent which can be adjusted to different values allowing for different versions of the model.

The SB calculations can be simplified through a series of Laplace transformations. Identifying the Laplace transformed mass spectrum as $G(\beta, \{\lambda\})$ and the term of input hadrons as $\varphi(\beta, \{\lambda\})$, then a bootstrap equation (BE) can be expressed as

$$\varphi(\beta, \{\lambda\}) = 2G(\beta, \{\lambda\}) - \exp[G(\beta, \{\lambda\})] + 1 \ . \tag{1}$$

*Work supported by the EPEAEK research funding program "Pythagoras I" (70/3/7315).

Equation (1) exhibits a singularity at the point $\varphi = \ln 4 - 1$. This Bootstrap singularity sets *boundaries* on the hadronic phase which is described by the set of the variables $(\beta, \{\lambda\})$. Real solutions of the BE can only exist for temperatures and fugacities that satisfy the constraint

$$\varphi(\beta, \{\lambda\}) \leq \ln 4 - 1 \, . \tag{2}$$

In the general form of SB several improvements can be made which allow for a better description of hadronic matter. The inclusion of all the known hadrons with masses up to 2400 MeV in the input term of the BE and also inclusion of strange hadrons is the first one. This leads to the introduction of the fugacities λ_s (strangeness fugacity) [5] and γ_s (partial strangeness equilibrium fugacity) [6]. Also different fugacities can be introduced for u and d quarks, allowing the description of systems which are not isospin symmetric [7]. The choice of the exponent α has important consequences, as every choice leads to a different physical behaviour of the system. An advantageous choice is $\alpha = 4$, since then a better physical behaviour is achieved as the system approaches the hadronic boundaries [5]. For $\alpha = 4$ the partition function can be written down and for point-like particles it assumes the form [5–7]

$$\ln Z_p(V, \beta, \{\lambda\}) = \frac{4BV}{\beta^3} \int_\beta^\infty x^3 G(x, \{\lambda\}) dx \equiv V f(\beta, \{\lambda\}) \, , \tag{3}$$

where B is the energy density of the vacuum (bag constant).

The contributions due to the finite size of hadrons, accounting for the repulsive interaction among hadrons, can be introduced via Van der Waals methodology [2,3], as well. The correct partition function avoids negative contributions to the volume. This requirement produces difficulties that can by surpassed by performing a Laplace transformation to the volume, an act which introduces the variable ξ. The new partition function is the pressure partition function [8]. If we are constrained to values $\xi > \xi_0$, where ξ_0 is the value of ξ corresponding to the thermodynamic limit ($V \to \infty$) and is found by

$$\xi_0 = f(\beta + \xi_0/(4B), \{\lambda\}), \tag{4}$$

then the pressure partition function can be evaluated without the need of Gaussian regularization [8] and the form it acquires is

$$\pi(\xi, \beta, \{\lambda\}) = \frac{1}{\xi - f(\beta + \xi/(4B), \{\lambda\})} \, , \tag{5}$$

where $f = \ln Z_p / V$.

The density and the pressure of the thermodynamic system can be obtained through the pressure grand canonical partition function (5)

$$\nu(\xi, \beta, \{\lambda\}) = \lambda \frac{\partial f(\beta + \xi/(4B), \{\lambda\})}{\partial \lambda} \left[1 - \frac{1}{4B} \frac{\partial f(\beta + \xi/(4B), \{\lambda\})}{\partial \beta} \right]^{-1} \, , \tag{6}$$

where λ is the fugacity corresponding to the particular density, and

$$P(\xi, \beta, \{\lambda\}) = \frac{1}{\beta} f(\beta + \xi/(4B), \{\lambda\}) \left[1 - \frac{1}{4B} \frac{\partial f(\beta + \xi/(4B), \{\lambda\})}{\partial \beta} \right]^{-1} \, . \tag{7}$$

Though volume is no longer an active variable of the system, it can be calculated for given baryon density ν_B (evaluated through (6)) and baryon number $\langle B \rangle$ which is a conserved quantity. The volume is retrieved through the relation $\langle V \rangle = \langle B \rangle / \nu_B$.

With the use of SB in order to describe interacting hadronic systems we can trace the possibility of a phase transition with the study of the pressure-volume isotherm curve. When this curve is calculated a region of instability is revealed. In fact, this curve has a part (near the boundaries of the hadronic domain) where pressure decreases while volume decreases also (see Fig. 1). Such a behaviour is a signal of a *first order phase transition*, which in turn can be mended with the use of a *Maxwell construction*.

This behaviour is due to the formation of bigger and bigger clusters as the system tends to its boundaries in the phase diagram. In that way the effective number of particles is reduced, resulting, thus, to a decrease of pressure. This is the basic mechanism that will produce a first order transition at lower temperatures and a critical point at finite density. To show that this instability in the $P - V$ curve is the result of the attractive part of the interaction included in the SB we shall calculate a similar curve using the Ideal Hadron Gas (IHG) model with Van der Waals volume corrections (repulsive part of interaction). The logarithm of the partition function of IHG (corresponding to (3)) is

$$f_{p\,IHG}(\beta, \{\lambda\}) = \frac{1}{2\pi^2 \beta} \sum_{\mathrm{a}} [\lambda_{\mathrm{a}}(\{\lambda\}) + \lambda_{\mathrm{a}}(\{\lambda\})^{-1}] \sum_i g_{\mathrm{a}i} m_{\mathrm{a}i} K_2(\beta m_{\mathrm{a}i}) \,, \tag{8}$$

where $g_{\mathrm{a}i}$ are degeneracy factors due to spin and isospin and "a" runs to all hadronic families. This function can be used in eq. (5) to calculate the Ideal Hadron Gas (IHG) pressure partition function in order to include Van der Waals volume corrections. The result is that the pressure is always found to increase as volume decreases, for constant temperature, allowing for no possibility of a phase transition.

The comparison of SB with the IHG (with volume corrections) for the same values of T and ξ is displayed in Fig. 1, where ν_0 is the normal nuclear density $\nu_0 = 0.14\ fm^{-3}$. In both cases (SB or IHG) the constraints $\langle S \rangle = 0$ (zero strangeness) and $\langle B \rangle = 2 \langle Q \rangle$ (isospin symmetric system, i.e. equal net numbers of u and d quarks) have been imposed. Also strangeness is fully equilibrated which accounts to setting $\gamma_s = 1$.

3. The Quark Matter partition function

For the thermodynamic description of the quark matter we shall use Lattice calculations of the pressure of the quark-gluon state which have been performed at finite chemical potential in [9], using an improved reweighting technique. The calculations are, though, carried out for rather heavy u, d quark masses. The quark-gluon pressure at $\mu_B = 0$ is plotted against the ratio of temperature to the transition temperature of quark matter at zero baryon chemical potential, $T/T_{0\,QGP}$, in Fig. 2 of [9]. The calculations for finite chemical potential are summarised in Fig. 3 of [9], where the difference of pressure at non-zero chemical potential and the pressure at zero chemical potential is plotted against $T/T_{0\,QGP}$ [9]. With the use of Figs. 2, 3 in [9], it is possible to calculate in principle the pressure of the quark-gluon phase at any temperature and baryon chemical potential and, thus, the partition function of the system in the grand canonical ensemble.

In order to have a complete description of the dependence of the pressure on the temperature and the chemical potential we use two sets of fitting functions. For constant

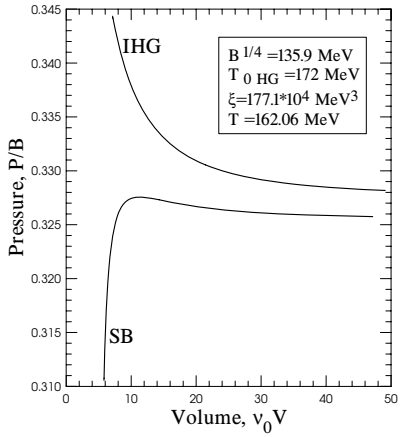

Figure 1. Pressure-volume isotherm curve for SB and IHG (both with Van der Waals volume corrections using the pressure ensemble).

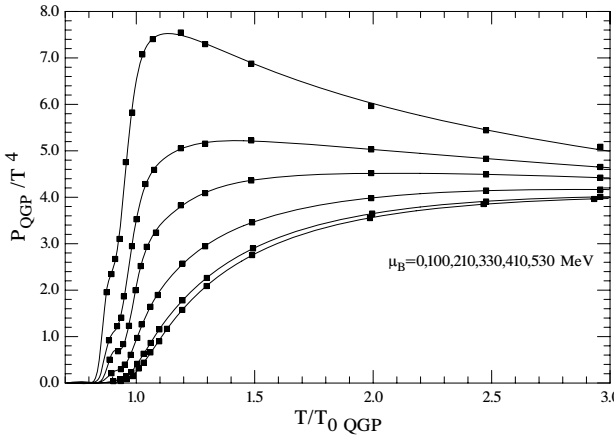

Figure 2. The pressure of the quark-gluon state divided by T^4 versus the ratio $T/T_{0\,QGP}$, for constant baryon chemical potential. The lines from bottom to top correspond to gradually increasing values of μ_B.

chemical potential the pressure as a function of $T/T_{0\,QGP}$ is fitted through

$$f(x) = \frac{a_1}{x^{c_1}\left[\exp\left(\frac{b_1}{x^{d_1}}\right)-1\right]^{f_1}} + \frac{a_2}{x^{c_2}\left[\exp\left(\frac{b_2}{x^{d_2}}\right)-1\right]^{f_2}}, \tag{9}$$

where a_i, b_i, c_i, d_i, f_i $(i = 1, 2)$ depend on μ_B, while for constant temperature the corresponding fit of the pressure as a function of μ_B is given by

$$g(x) = a + b\exp(cx^d), \tag{10}$$

where a, b, c, d depend on the temperature ratio $T/T_{0\,QGP}$. Performing fitting procedures we are able to evaluate the partition function, as well as, its derivatives with respect to μ_B and T at any given point.

In Fig. 2 we have reproduced the quark-gluon pressure as a function of the temperature for constant baryon chemical potential. The squares are points directly measured from the graphs of [9], while the lines represent the calculation with our fits on these points.

4. The critical point in the phase diagram

Having descriptions for both the hadronic and the quark phase we can search for a transition between the two phases. First we have to deal with the free parameters that exist in our models. In [9], where the results of the pressure is presented, the transition temperature of the quark state at zero density ($T_{0\,QGP}$) is not fixed. In [10], however, the QCD critical point is studied with quark mass input values closer to the physical ones and a zero-density temperature $T_{0\,QGP} = 164 \pm 3$ MeV. Therefore in what follows, we choose

$$T_{0\,QGP} = 164\ MeV\ . \tag{11}$$

As far as the hadronic phase is concerned, an upper bound for the parameter $T_{0\,HG}$ can be fixed at the value 183 MeV. This temperature allows for the best matching of the strange chemical potential μ_s between the hadronic and the QGP phase [5]. So we shall set

$$T_{0\,HG} \leq 183 \text{ MeV}. \tag{12}$$

The fact that $T_{0\,HG}$ and $T_{0\,QGP}$ acquire different values does not imply a contradiction. At $\mu_B = 0$ the strongly interacting system belongs to the crossover regime where the quark and hadron phases are indistinguishable.

Turning now our attention to ξ, we adopt $\xi > \xi_0$ (ξ_0 given by (4)) in order to have always a real pressure partition function. For simplicity we also choose to have $\xi = const.$ for every set of $(T, \{\lambda\})$. Since the value of ξ at the thermodynamic limit, ξ_0, depends on the choice of thermodynamic variables, we have to locate the specific set that gives us the highest value of ξ_0. It is found that the greatest value of ξ_0 corresponds to $T = T_{0\,HG}$ and consequently $\{\lambda\} = \{1\}$. So in order to have a real pressure partition function for a constant value of ξ all over the space of our thermodynamic variables it suffices to require

$$\xi > \xi_0(T_{0\,HG}, \{\lambda\} = \{1\}) \, . \tag{13}$$

Finally, as a consistency requirement on the thermodynamics of lattice QCD [10,11] and bootstrap matter, we impose the constraint

$$T_{cr.p.} < T_{0\,QGP} \, . \tag{14}$$

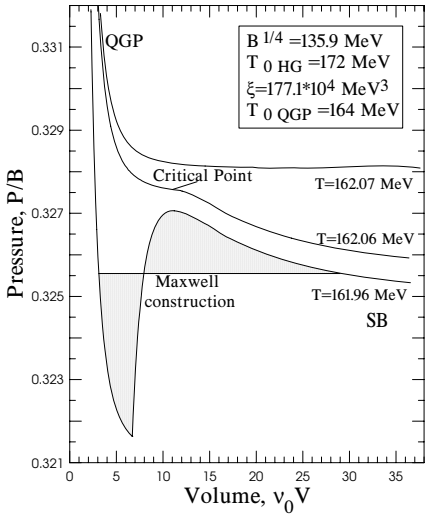

Figure 3. Three isotherm pressure-volume curves for Hadron Gas (using SB) and QGP phase (using the lattice pressure of [9]). The low temperature isotherm needs Maxwell construction, the middle temperature isotherm develops a critical point and the high temperature isotherm corresponds to crossover.

Then, if the values for the free parameters are chosen, within the above constraints, one may calculate for a specific temperature the pressure isotherms of Hadron Gas and QGP. Assuming that the baryon number is a conserved quantity to both phases, the equality of volumes is equivalent to the equality of baryon densities. The graph of the pressure-volume isotherm can be drawn using the plot of pressure against the inverse baryon density.

Tracing the point where the isotherms of two phases meet, we find that at a low temperature the intersection of QGP and SB pressure-volume isotherms takes place at a location where the Hadron Gas pressure is decreasing while volume decreases. The resulting pressure-volume curve includes an unstable part which has to be repaired through a suitable Maxwell construction. This curve includes a region where a first-order transition takes place. As the temperature increases, there exists a value for which the QGP and SB isotherms meet at a point where the Hadron Gas pressure has a maximum. In that case no Maxwell construction is needed and since this point is located at finite volume or not zero baryon density (equivalently not zero chemical potential) it can be associated with the QCD critical point. As temperature rises more, the resulting pressure-volume isotherm also increases, while volume decreases, without the need of a Maxwell construction and the situation belongs to the crossover region. A graph that summarises the situations met in the pressure volume isotherms of hadronic and quark systems in the neighbourhood of the critical point is Fig. 3.

To locate the critical point numerically with the use of the lattice partition function, for given parameters ξ, $T_{0\,HG}$ and $T_{0\,QGP}$, the conditions have to be determined for which the SB pressure is equal to the QGP pressure at the same volume, corresponding to the maximum SB pressure. Setting the fugacity of partial strangeness equilibrium $\gamma_s = 1$ a hadronic state is characterised by the set of thermodynamic variables $(T, \lambda_u, \lambda_d, \lambda_s)$, while a quark-gluon state evaluated on the lattice [9] is characterised by the two variables (T, λ'_q). The u and d quarks are characterised by the same fugacity $\lambda'_u = \lambda'_d = \lambda'_q = \lambda'^{1/3}_B$. To evaluate the unknown variables we have to solve the following set of equations

$$\nu_{B\,SB}(T, \lambda_u, \lambda_d, \lambda_s) = \nu_{B\,QGP}(T, \lambda'_q) \tag{15}$$

$$P_{SB}(T, \lambda_u, \lambda_d, \lambda_s) = P_{QGP}(T, \lambda'_q) \tag{16}$$

$$\left.\frac{dP_{SB}(T, \lambda_u, \lambda_d, \lambda_s)}{dV}\right|_{T=const} = 0 \tag{17}$$

$$\langle\, S \,\rangle_{SB}\,(T, \lambda_u, \lambda_d, \lambda_s) = 0 \tag{18}$$

$$\langle\, B \,\rangle_{SB}\,(T, \lambda_u, \lambda_d, \lambda_s) - 2\ \langle\, Q \,\rangle_{SB}\,(T, \lambda_u, \lambda_d, \lambda_s) = 0 \tag{19}$$

The area in the (T, μ_B) plane which gives solutions for the critical point compatible with the constraints (11)-(14) is depicted as shaded area in Fig. 4.

Recent lattice QCD studies offer, apart from the quark-gluon pressure which has been a basic ingredient in our approach, important results on the existence and location of the critical point itself. In [11] the critical point is found to reside at $T_{cr.p.} = 160 \pm 3.5$ MeV and $\mu_B = 725 \pm 35$ MeV, with $T_{0\,QGP} = 172 \pm 3$ MeV. These calculations have the drawback that have been performed with u and d quark mass which has a value about four times the physical value. Improved calculations have been performed in [10], where the light quark masses have decreased by a factor of 3 down their physical values. The critical point is found now (with $T_{0\,QGP} = 164 \pm 3$ MeV) to be at $T_{cr.p.} = 162 \pm 2$ MeV and $\mu_B = 360 \pm 40$ MeV. This point is depicted on Fig. 4 with the full star and it falls completely inside the compatible domain of the critical point, according to our calculations.

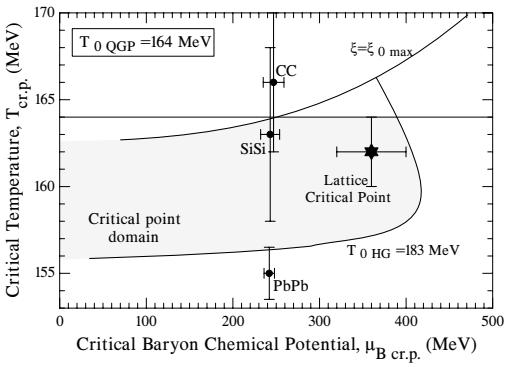

Figure 4. Domain in the (T, μ_B) plane (shaded area) which is compatible with solutions for the position of the critical point. There are, also, displayed the freeze-out points from NA49 at 158 AGeV [12] and the lattice calculated critical point from [10].

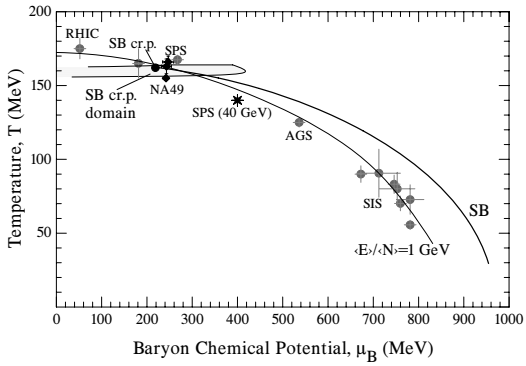

Figure 5. Comparison of the positions of our critical point solutions presented in Fig. 4, with the freeze-out points from different experiments and the freeze-out curve of $\langle E \rangle / \langle N \rangle = 1$ GeV.

In Fig. 5 we illustrate a representative solution for the critical point, as well as for the QGP-hadron transition line from those which are included in the shaded area of Fig. 4 on the (T, μ_B) plane. The chosen critical point is associated with $T_{0\,HG} = 172$ MeV, while the rest of the parameters are those of Fig. 3. It is located at $T_{cr.p.} = 162.1$ MeV and $\mu_B = 218.7$ MeV. The full circle represents our solution for the critical point. This circle is the endpoint of the solid thick line representing the bootstrap calculation of the maximum hadronic pressure, which is close to the first order critical line. In Figs. 4-5 we compare our solutions for the critical point with the freeze-out points from different experiments. We depict freeze-out points from NA49 at 158 AGeV [12] for systems of different size (C+C, Si+Si, Pb+Pb) that fall inside the compatible domain of the critical point, if the errors in their determination are taken into account. These experiments are interesting since they could trace critical fluctuations associated with a critical point of second order [13]. In Fig. 5 the comparison is extended to a larger number of experiments. On the same graph we have also depicted the curve of $\langle E \rangle / \langle N \rangle = 1$ GeV [14] that fits freeze-out points which are spread to a wide region of the phase diagram. It is evident that our calculations set the critical point to a location easily accessible by experiments, especially by CERN/SPS.

5. Conclusions

Statistical bootstrap, which describes the hadronic phase more accurately than the ideal Hadron Gas by including the attractive part of the interaction among hadrons, exhibits an instability in the pressure-volume isotherm which can be connected with a first order phase transition.

The pressure of the quark-gluon phase is available from the lattice, despite the fact that unphysical values of the light quark masses are still involved. The lattice partition

function of the quark-gluon phase and the necessary derivatives can be calculated through suitable techniques.

The joining of the SB and the lattice partition function for the hadronic and the quark state respectively, allows for the determination of a critical point at finite baryon chemical potential which can be related to the critical point of QCD.

Setting the free parameters in our model in a way to fulfil certain constraints we are left with a compatible domain in the (T, μ_B) plane for the location of the critical point. Recent lattice calculations [10] drive the critical point within the domain of our solutions. It is interesting that the current location is situated in the (T, μ_B) plane in a region easily accessible by the freeze-out conditions of experiments at the CERN/SPS.

REFERENCES

1. F. Wilczek, Proc. Banff 1999, Theoretical physics at the end of the twentieth century, Springer-Verlag 2002, p.567, Edited by Yvan Saint-Aubin and Luc Vinet; J. Berges and K. Rajagopal, Nucl. Phys. B 538 (1999) 215; M.A. Halasz, A.D. Jackson, R.E. Shrock, M.A. Stephanov and J.J. Verbaarschot, Phys. Rev. D 58 (1998) 096007.
2. N.G. Antoniou and A.S. Kapoyannis, Phys. Lett. B 563 (2003) 165; N.G. Antoniou, F.K. Diakonos and A.S. Kapoyannis, Proc. 10th International Workshop on Multiparticle Production, Crete, Greece 8-15 June 2002, World Scientific 2003, p.201, Edited by: N.G. Antoniou, F.K. Diakonos and C.N. Ktorides.
3. N.G. Antoniou, F.K. Diakonos and A.S. Kapoyannis, Nucl. Phys. A 759 (2005) 417.
4. R. Hagedorn, Suppl. Nuovo Cimento III (1965) 147; Suppl. Nuovo Cimento VI (1968) 311; Nuovo Cimento LVI A (1968) 1027; R. Hagedorn and J. Rafelski, Phys. Lett. B 97 (1980) 136.
5. A.S. Kapoyannis, C.N. Ktorides and A.D. Panagiotou, J. Phys. G 23 (1997) 1921; Phys. Rev. D 58 (1998) 034009.
6. A.S. Kapoyannis, C.N. Ktorides and A.D. Panagiotou, Phys. Rev. C 58 (1998) 2879.
7. A.S. Kapoyannis, C.N. Ktorides and A.D. Panagiotou, Eur. Rhys. J. C 14 (2000) 299; J. Phys. G 28 (2002) L47.
8. R. Hagedorn, Z. Phys. C 17 (1983) 265.
9. Z. Fodor, S.D. Katz and K.K. Szabo, Phys. Lett. B 568 (2003) 73.
10. Z. Fodor and S.D. Katz, JHEP 0404 (2004) 050.
11. Z. Fodor and S.D. Katz, JHEP 0203 (2002) 014; talk given at Finite Density QCD at Nara, Nara, Japan, 10-12 July 2003, Prog. Theor. Phys. Suppl. 153 (2004) 86.
12. F. Becattini, M. Gazdzicki, A. Keranen, J. Manninen and R. Stock, Phys. Rev. C 69 (2004) 024905; F. Becattini, J. Manninen and M. Gazdzicki, hep-ph/0511092.
13. N.G. Antoniou, Y.F. Contoyiannis, F.K. Diakonos and G. Mavromanolakis, Nucl. Phys. A 761 (2005) 149; N.G. Antoniou, Y.F. Contoyiannis, F.K. Diakonos, A.I. Karanikas and C.N. Ktorides, Nucl. Phys. A 693 (2001) 799.
14. J. Cleymans and K. Redlich, Phys. Rev. Lett. 81 (1998) 5284.